

PULSAR X-RAY AND GAMMA-RAY PULSE PROFILES: CONSTRAINT ON OBLIQUITY AND OBSERVER ANGLES

Alice K. Harding and Alexander G. Muslimov ¹

Laboratory for High Energy Astrophysics
NASA/Goddard Space Flight Center, Code 661
Greenbelt, MD 20771 USA

harding@twinkie.gsfc.nasa.gov; muslimov@lhea1.gsfc.nasa.gov

ABSTRACT

We model the thermal X-ray profiles of Geminga, Vela and PSR 0656+14, which have also been detected as γ -ray pulsars, to constrain the phase space of obliquity and observer angles required to reproduce the observed X-ray pulsed fractions and pulse widths. These geometrical constraints derived from the X-ray light curves are explored for various assumptions about surface temperature distribution and flux anisotropy caused by the magnetized atmosphere. We include curved spacetime effects on photon trajectories and magnetic field. The observed γ -ray pulse profiles are double peaked with phase separations of 0.4 - 0.5 between the peaks. Assuming that the γ -ray profiles are due to emission in a hollow cone centered on the magnetic pole, we derive the constraints on the phase space of obliquity and observer angles, for different γ -ray beam sizes, required to produce the observed γ -ray peak phase separations. We compare the constraints from the X-ray emission to those derived from the observed γ -ray pulse profiles, and find that the overlapping phase space requires both obliquity and observer angles to be smaller than $20 - 30^\circ$, implying γ -ray beam opening angles of at most $30 - 35^\circ$.

Subject headings: pulsars: emission mechanisms: gamma-rays: general:
X-rays — pulsars: individual: Geminga, Vela, PSR 0656+14 — stars:
neutron

Submitted to *The Astrophysical Journal*.

¹NRC/NAS Senior Research Associate

1. INTRODUCTION

The multifrequency observations of γ -ray pulsars may potentially constrain the geometry and location of emission regions in a neutron star (NS) magnetosphere. Such a constraint is necessary for our understanding of the entire picture of pulsar emission in different energy bands. However, in practice, the interpretation of high-energy observations is rather ambiguous and involves a number of model assumptions. The recent X-ray observations of pulsars Geminga, Vela, and PSR 0656+14 seem to indicate that the pulsed emission has a two-component X-ray spectrum (Ögelman 1995, Halpern & Wang 1997, Strickman, Harding, & De Jager 1998), where the soft (pulsed) component is likely due to thermal emission. Theoretical work by Pavlov et al. (1994) has shown that X-ray pulsation reaching the observed pulsed fractions can result from anisotropic emission in a magnetized atmosphere, even when the entire NS surface radiates. If this interpretation is correct, then the peak in the soft thermal X-ray profile is near the phase of closest approach to the magnetic pole. It is thus interesting to explore the relation between X-ray profiles as thermal black-body emission from the whole stellar surface “beamed” along the magnetic field in a NS atmosphere and non-thermal pulsed γ -ray emission from these pulsars generated in the innermost magnetosphere of a NS (polar cap model)(Harding & Muslimov 1997a). The polar cap models for pulsed gamma-ray emission (Daugherty & Harding 1996, Sturmer & Dermer 1994) predict double-peaked pulse profiles, where the closest approach to the pole is centered between the pulses. The peak of the broad thermal X-rays profile should thus also occur between the two gamma-ray pulses.

In this paper we model the soft X-ray and γ -ray light curves for the pulsars Geminga, Vela, and PSR 0656+14 surveying all possible orientations (see Figure 1) between the magnetic and spin axes (referred to as the **obliquity** angles) and the angle between the observer’s line of sight and spin axis (referred to as the **observer** angles). In our modeling of the X-ray and γ -ray light curves we assume that the NS has a centered dipole-like surface magnetic field, and that the thermal flux from the stellar surface corresponds to that expected in a cooling NS of age $\sim 10^4 - 3 \times 10^5$ yr (the age category of Geminga, Vela and PSR 0656+14). In our analysis of the main observational features we consciously avoid additional model assumptions such as the possibility of polar cap heating by the precipitating relativistic particles and γ -rays, off-setting of the magnetic axis of the NS and/or the presence of higher-order multipoles on the stellar surface (which are not unreasonable at all for future modeling), and occurrence of any specific cooling scenario (e.g. such as those with internal heating of the NS, or those allowing for any of the countless variants of rapid or slow cooling, etc). Also, we have not considered very compact NS models for which the effects of strong gravity by themselves may result in quite interesting signatures (Shibanov et al 1995). All these possibilities, being attractive for a theoretical

study, are rather abstract when discussed in the context of the currently available X-ray and γ -ray observational data on pulsars. The quality of the observations and also the complexity of theoretical modeling (which usually involves many free parameters and poorly justified model assumptions) do not allow any conclusive statement regarding any of the abovementioned possibilities.

The main goal of our study is to demonstrate that a polar cap model for the interpretation of the γ -ray emission is viable at least for Geminga, Vela, and PSR 0656+14, and that the main observed X-ray and γ -ray pulse characteristics (X-ray pulsed fraction, half-width of the X-ray profile, phase separation of γ -ray peaks, and a phase shift $\sim 0.1 - 0.2$ between the γ -ray peaks) for these pulsars can be understood within the framework of a standard NS model with a dipole-like magnetic field and a relatively small obliquity ($\lesssim 30 - 35^\circ$). We begin our paper (§ 2) with a summary of the observational X- and γ -ray data on pulsars Geminga, Vela, and PSR 0656+14. In § 3 we describe the details of our modeling of the observed soft X- and γ -ray emission, and in § 4 we present the results of our numerical calculations. Our principal conclusions are summarized in § 5.

2. SUMMARY OF THE OBSERVATIONAL DATA

In Figure 2 we show soft X-ray and high-energy γ -ray pulse profiles for Geminga, Vela and PSR 0656+14. We have chosen these sources for modeling X-ray and γ -ray pulsed profiles because they have been identified as having well-defined thermal components. Recent hard X-ray observations of Geminga (Halpern & Wang 1997) and PSR 0656+14 (Greiveldinger et al. 1996) with ASCA and Vela with RXTE (Rossi X-ray Timing Explorer; Strickman, Harding & De Jager 1998) have clearly defined the existence of separate non-thermal components and therefore greatly strengthened the interpretation of the soft X-ray components seen by ROSAT as thermal in origin. ROSAT observations of these sources had revealed phase shifts between the pulses seen in low energy (0.1 – 0.5 keV) and high energy bands (0.5 – 2.0 keV). Better definition of the pulse profile and spectrum in the energy range 1.0 - 30. keV by ASCA and RXTE have shown that, in the case of Vela and Geminga, the high energy pulses are double-peaked and in phase with the γ -ray pulses measured by EGRET. Furthermore, the 2.0 - 30 keV spectrum of Vela is consistent with an extrapolation of the OSSE spectrum (Strickman et al. 1998). The characteristics of the hard X-ray components in these pulsars are therefore best explained if their origin is non-thermal magnetospheric emission. The phase shifts between the hard and soft components seen by ROSAT may be understood as a transition from a single broad thermal profile to a double-peaked non-thermal profile.

The measured pulsed fractions and pulse widths are strongly energy dependent. The pulsed fraction (defined in equation [7]) of Geminga and PSR 0656+14 increases through the ROSAT band, starting at about 10 – 20% around 0.1 keV and reaching 80 – 90% above 1 keV. But it is not clear how much of this increase is intrinsic to the thermal component and how much is due to contamination by the hard, non-thermal component, which is known to have a high pulsed fraction. In the case of Geminga (Halpern & Wang 1997), the pulse profile also changes significantly above about 0.5 keV, where the power law spectral component becomes significant, indicating pulsed fraction contamination by the non-thermal component at the higher ROSAT energies. We have therefore chosen to model the thermal X-ray pulse profiles only in the lowest energy ROSAT bands available. For the purposes of our modeling, we have taken the observed pulse fractions of 20 – 30% for Geminga, based on the observed profiles given by Halpern & Wang (1997) for the range 0.08 - 0.28 keV. Table 1 summarizes the observed parameters of the X-ray and γ -ray emission that are relevant to our modeling. The observed pulsed fractions for Vela and PSR 0656+14 are 11% (Ögelman, Finley, & Zimmerman 1993) and 7% (Finley, Ögelman, & Kiziloğlu 1992, Finley 1997, Anderson et al. 1993), respectively. The pulse widths (FWHM – Full Width at Half Maximum) in the lowest energy bands for all these pulsars lie roughly between 0.35 and 0.5 of pulse phase. We have determined approximate pulse widths, from the definition given in § 4, of 0.35 ± 0.05 for Geminga, 0.45 ± 0.05 for Vela, and 0.55 ± 0.05 for PSR0656+14.

Vela and Geminga have well-defined high-energy γ -ray profiles, as seen by EGRET, showing two sharp peaks with phase separations of 0.4 and 0.5 respectively and emission between the peaks (Kanbach et al. 1994, Meyer-Hasselwander et al. 1994). PSR 0656+14, however, is considered only as a possible detection of pulsed emission by EGRET, with a poorly defined γ -ray profile (Ramanamurthy et al. 1996). For this study, we will assume a double-peaked profile with phase separation of 0.4, but we emphasize that this is highly uncertain. The relative phases of the X-ray and γ -ray profiles are reasonably well determined for Vela and Geminga, but very uncertain for PSR 0656+14. The absolute phase was not determined at the time of the ROSAT measurement (Finley, Ögelman, & Kiziloğlu 1992), but we have taken in Figure 2 the relative phase between the EGRET and soft ROSAT profiles as determined by Thompson (1997) from comparison of EGRET, ASCA (both having absolute timing) and hard ROSAT profiles. For all three pulsars, the broad X-ray profiles roughly coincide in phase with the γ -ray profile. The peaks in the X-ray profile lie between the γ -ray peaks in the case of Geminga and Vela, although both are offset by about 0.1 in phase toward the second γ -ray peak.

3. DESCRIPTION OF THE MODEL

In our modeling of the (soft) thermal X-ray emission from a NS surface we include the effect of general-relativistic light bending which effectively smears out any intrinsic flux variation with pulsar rotational phase. Thus, the strong gravity of the NS tends to decrease the pulsed fraction, while the pulse width tends to increase (cf. Page 1995). Much of the details of isotropic thermal X-ray emission from a NS surface have been discussed by Page (1995; and references therein), who concluded that the observed pulse fraction of Geminga’s X-ray emission is difficult to explain unless the pulsar obliquity is close to $\pi/2$ and the surface magnetic field of the NS is highly non-dipolar. The available X- and γ -ray observational data on Geminga, Vela, and PSR 0656+14 summarized in § 2 prompted us to explore the effect of X-ray beaming on the (supposedly) thermal soft X-ray emission from these pulsars.

It is generally expected (see discussion and references below) that the magnetic polar caps of a cooling NS are slightly hotter than the rest of the stellar surface, because of the effect of the strong magnetic field on heat transport in the surface layers of the NS. Hence, even an isotropically emitting NS surface may look somewhat brighter at the phases when the photons emitted from the polar caps get beamed into the observer’s viewing angle. The presence of an intrinsic anisotropic component (e.g. associated with the anisotropy of radiative transfer in a strong magnetic field) may substantially enhance a contrast between fluxes received at the pole and the equator. The beaming of the X-ray emission along the magnetic field, as will be discussed in this paper, may allow a relatively large pulsed fraction even for a small obliquity and for a dipolar stellar magnetic field.

We assume that the γ -ray emission is generated above the pulsar polar cap within ~ 1 -3 stellar radii from the surface. The mechanism for γ -ray production from the polar cap is a curvature-synchrotron/pair cascade from electrons accelerated in a region of open magnetic field lines above a polar cap (see Daugherty & Harding 1996 for details). The efficiency of the electron-positron pair and γ -ray production varies across this region, so that in an axisymmetric case the emission is peaked in a hollow cone inscribed in the surface formed by the last open field lines. The two narrow γ -ray peaks with interpeak emission observed in Geminga and Vela are well reproduced in such a “hollow-cone” model.

The calculation of the photon flux in a gravitational field of a slowly rotating NS is rather straightforward and has been described by many authors (see e.g. Pechenick, Ftaclas, & Cohen 1983, Riffert & Mészáros 1988, and Page 1995 for the most recent relevant discussions), and we shall not reproduce it in our paper. We must note however, that because of general-relativistic light bending the specific flux is now a first moment of specific intensity with respect to $\cos\theta^*$, where θ^* is an angle between the photon wave vector and

the local normal at the stellar surface, and the integration should be now taken over a solid angle ($> 2\pi$ steradian) determined by the maximum deflection angle (see e.g. Page 1995) of a photon emitted nearly tangential to the surface. Note that in our calculations this angle (see §§ 3.1 and 3.3), which is counted from the local normal at the emission point, is 131.9° .

3.1. Thermal X-Ray Emission

We consider thermal black-body X-ray emission from the whole stellar surface, including the effects of general-relativistic light bending and anisotropization of emission produced by a dipolar surface magnetic field.

It is important that the effect of a strong magnetic field on the X-ray emission is twofold:

1. anisotropy of the surface temperature distribution: the transverse heat conductivity is suppressed due to magnetization of electrons, which results in a surface temperature at the magnetic pole that is e.g. a factor of 1.5-2.5 higher than at the magnetic equator;
2. beaming of the thermal emission along a tangent to the magnetic field lines in a strongly magnetized atmosphere (when $h\nu_c \gg kT$, where $\nu_c = eB/2\pi m_e c$ is the electron cyclotron frequency in a magnetic field of strength B).

The effect of beaming of the emission results from the angle and polarization dependent opacity in a NS atmosphere, that is lower along the magnetic field than in the transverse direction. The reduction of the photon opacity in the magnetic field of a NS was first discussed by Cohen et al. (1970) and Tsuruta et al. (1972), and addressed in more detail by Lodenquai et al. (1974). These authors found that (see Lodenquai et al. 1974) in a magnetized plasma two independent modes (ordinary and extraordinary modes) of an electromagnetic wave have significantly different mean free paths. For example, the extraordinary-mode photons (for which the electric field wavevector is perpendicular to the magnetic field) generally have a much longer mean free path than ordinary-mode photons and give the main contribution to radiation transport in the very surface layers of a NS atmosphere. Lodenquai et al. (1974) have presented the approximate relation between scattering cross-sections with and without strong magnetic field (e.g. $\gtrsim 10^{12}$ G) for the

extraordinary mode:

$$\sigma_{\perp}(\mathbf{B}) \approx \left(\frac{\omega}{\omega_c}\right)^2 \sigma(0), \quad \omega \ll \omega_c \equiv 2\pi\nu_c. \quad (1)$$

where ω is the frequency of a photon.

Many authors have since calculated the radiative thermal conductivities in a plasma with a magnetic field (see e.g. Pavlov & Yakovlev 1977, Silant'ev & Yakovlev 1980, and references therein) and have discussed in more details the effects of opacity on the emerging emission from a magnetized atmosphere of a NS (see e.g. Kaminker, Pavlov & Shibarov 1982, and Pavlov et al. 1994).

The anisotropy of the surface temperature distribution due to anisotropy of electron thermal conduction in a strong magnetic field ($\sim 10^{12} - 10^{13}$ G) in a NS crust can be adequately described by an approximate formula (see Greenstein & Hartke 1983):

$$T_*(\Theta) = T_p(\cos^2 \Theta + \chi_0^4 \sin^2 \Theta)^{1/4}, \quad (2)$$

where T_p is the effective temperature at the magnetic pole, Θ is the angle between the local normal to the surface and tangent to the field line, $\chi_0 = T_{\text{eq}}/T_p \approx 0.3 - 0.6$, T_{eq} is the effective temperature at the magnetic equator. The parameter χ_0 can be expressed in terms of the physical quantities as $\chi_0 = (\kappa_{\perp}/\kappa_{\parallel})^{1/4}$, where κ_{\parallel} and κ_{\perp} are the thermal conductivities in the surface layers of a NS along and perpendicular to the direction of a magnetic field, respectively. The values of χ_0 can be estimated from the dependences between the surface and internal temperatures of a cooling NS calculated for the range of magnetic fields $\leq 10^{10} - 10^{14}$ G and presented by Page (1995, Figure 1). However, the results of our calculations are rather insensitive to the particular value of χ_0 we choose from the range specified above. The effect of anisotropic cooling and atmospheric radiation of neutron stars with strong magnetic fields have been discussed by Shibarov et al. (1995, see also references therein). In our calculation we assume a dipole magnetic field modified by the static part of the gravitational field (see e.g. Muslimov & Tsygan 1987).

In our analysis, to incorporate the effect of X-ray beaming, we exploit the results of the numerical calculations of radiative transfer from a magnetized atmosphere of a NS (Zavlin et al. 1995) which indicate that the emission pattern consists of a peaked (along the direction of the magnetic field) pencil beam component and a broad, nearly isotropic, fan beam component. In Figure 3 we present the normalized profiles of the function $I_{\nu}(\theta_B) \cos(\theta_B)$ we use in our calculations, where I_{ν} is the specific intensity of radiation, and θ_B is the angle between the wave vector and tangent to a magnetic field line at the stellar surface. These profiles represent two examples having beamed components of different shapes: narrow and weak, and broad and strong. They correspond to the relatively low

(~ 0.18 keV) and high (~ 1 keV) photon energies and are very similar to those provided by Zavlin, Shibano & Pavlov (1995) in Figures 2a and 2b, respectively (that are calculated for the stellar effective temperature of 3×10^6 K and surface value of the magnetic field strength of $\sim 10^{12}$ G). We must note that these angular profiles are generally energy dependent and for different parameters may look different. For example, the relative magnitude of the beamed component increases with photon energy and also with an increase in surface gravity. Qualitatively, as has been discussed by Zavlin, Shibano & Pavlov (1995), the beamed component which is determined by the enhanced atmospheric transparency along the magnetic field, corresponds to the photons emerging from the deeper and hotter layers along the field, and the dependence on the surface gravity results from the emerging radiation dependence on the temperature scale height.

We calculate the X-ray flux received by a distant observer using the following expression (cf. Page 1995)

$$F_\nu(E, T, \alpha, \zeta) = F_0 \int_0^{\theta_{\max}} \int_0^{2\pi} I_\nu(E_*, T_*, \theta_B) \cos[\theta^*(\theta)] \sin \theta d\theta d\phi, \quad (3)$$

where E and T are the red-shifted energy of a photon and stellar effective temperature, respectively, E_* and T_* are the photon energy and stellar effective temperature as measured at the stellar surface, α and ζ are the obliquity and observer angle, respectively, F_0 is a normalization constant, θ and ϕ are the angles of a spherical coordinate system with the axis along the local normal at the point of photon emission, $\theta_{\max} = 131.9^\circ$ is the maximum angle between the normal at the point of photon emission and the wave vector of a photon received by the observer, $\theta^*(\theta)$ is the angle between the photon wave vector and the local normal at the stellar surface. The relation between the angle θ^* and angle θ , at which the photon reaches the observer, is defined by (see e.g. Pechenick, Ftaclos, & Cohen 1983 for details)

$$\theta(\theta^*) = a \int_0^\varepsilon \frac{dx}{\sqrt{1 - (1 - x)x^2 a^2}}, \quad (4)$$

where $a = \sin \theta^*/[\varepsilon(1 - \varepsilon)^{1/2}]$, $\varepsilon = r_g/R$ and $r_g = 2GM/c^2$ is the gravitational radius of a NS of mass M and radius R .

3.2. Non-thermal Gamma-Ray Emission

Most of the observed γ -ray pulsars have double-peaked profiles with peak phase separations of 0.4 - 0.5 (Thompson 1996). There are presently two types of pulsar γ -ray

emission models which have been studied in detail. Polar cap models consider electrostatic acceleration above the neutron star surface near the magnetic poles, arising from charge starvation caused by field line curvature (Arons 1983) and general relativistic inertial frame dragging (Muslimov & Tsygan 1992, Muslimov & Harding 1997). The γ -ray emission in polar cap models (Daugherty & Harding 1994, Daugherty & Harding 1996; Sturmer & Dermer 1994) is a hollow cone, with opening angle θ_γ , centered on the magnetic pole (see Figure 1), producing either double-peaked or single-peaked pulse profiles depending on observer orientation. Outer gap models consider acceleration in the outer magnetosphere in “Holloway” gaps caused by charge depletion along the null charge surfaces (Cheng, Ho & Ruderman 1986). The γ -ray emission pattern is a curved fan beam described by the last open magnetic field line (Romani & Yadigaroglu 1995). Both models can produce double-peaked γ -ray profiles similar to what is observed, but the phase of the magnetic pole relative to the two γ -ray peaks is very different in the two types of model. For the polar cap models, the phase of closest approach to the magnetic pole, and thus the peak of the thermal X-ray pulse, lies midway between the γ -ray peaks, in the interpeak emission region. In the outer gap models, the predicted phase of closest approach to the magnetic pole and the thermal X-ray pulse lies outside the γ -ray peaks.

In this paper, we consider the hollow-cone γ -ray beam pattern predicted by polar cap models. When $\theta_\gamma \sim \alpha$, an observer may see a broad double-peaked γ -ray pulse profile with the peak separation $\Delta\phi$ given by (Daugherty & Harding 1994)

$$\cos(\Delta\phi) = \frac{\cos\theta_\gamma - \cos\alpha \cos\zeta}{\sin\alpha \sin\zeta}, \quad (5)$$

where θ_γ is the γ -ray beam opening angle. The γ -ray beam opening angle is determined approximately by the locus of the tangent to the outermost open field line:

$$\tan\theta_\gamma \simeq \frac{3\theta_{\text{pc}}(1 - \theta_{\text{pc}}^2 r/R)^{1/2}(r/R)^{1/2}}{3(1 - \theta_{\text{pc}}^2 r/R) - 1} = \frac{3}{2} \left(\frac{\Omega r}{c}\right)^{1/2} \frac{(1 - r/R_{\text{LC}})^{1/2}}{(1 - 3r/2R_{\text{LC}})}, \quad (6)$$

where θ_{pc} is the polar cap half-angle, r is the radius of emission, R is the stellar radius, Ω is the angular velocity of stellar rotation, and $R_{\text{LC}} \equiv c/\Omega$ is the light-cylinder radius. In this formula the equality holds for the standard value of the polar cap half-angle, $\theta_{\text{pc}} = (\Omega R/c)^{1/2}$. If $r > R$ and/or the polar cap half-angle is larger than the standard value, then θ_γ could be as large as $20^\circ - 30^\circ$ (Figure 1). General relativistic effects on the photon trajectory and on the dipole magnetic field structure introduce small corrections to θ_γ and θ_{pc} .

For an observed phase separation $\Delta\phi$ between the first and second peaks of the γ -ray pulse profile, equation (5) describes closed contours in the $\zeta - \alpha$ plane, as a function of θ_γ .

Such contours for Vela ($\Delta\phi = 0.4$) and Geminga ($\Delta\phi = 0.5$) are shown as dashed lines in Figures 6 and 7, for values of θ_γ between 5° and 35° . In the case of $\Delta\phi = 0.5$ the contours collapse to single lines, so that the relation between ζ and α is single-valued. The predicted γ -ray beam opening angles θ_γ (see e.g. Daugherty & Harding 1996) from equation (6) are between $\sim 2^\circ - 20^\circ$ for Geminga ($\Omega = 26.5 \text{ s}^{-1}$) and between $\sim 3^\circ - 35^\circ$ for Vela ($\Omega = 70.6 \text{ s}^{-1}$), for $r = (1 - 3)R$ and θ_{pc} up to 5 times the standard value. Therefore, small values of both ζ and α ($< 35^\circ$) are favored in polar cap models.

3.3. Main Input Parameters

We use a canonical NS model of mass $1.4 M_\odot$ and radius of 10 km. Note that for this stellar model a photon emitted almost tangential to the stellar surface gets deflected (while remaining in the same plane with a tangent to the trajectory and the normal to the stellar surface at the point of emission) by an angle of 131.9° to the normal. We must point out that the canonical NS model is consistent with the recent RXTE results by the Illinois group (Miller, Lamb & Psaltis 1997) which constrain NS equation of state (admittedly for NSs in Low-Mass X-ray Binaries rather than for isolated NSs).

In Figure 3 we show two characteristic emission patterns for the beamed surface X-ray emission we have used in our calculations. In general, the intensity of this beamed emission can be presented as a linear combination of the pencil and fan components. In this paper we have chosen a particular sample (see Figure 3) consistent with the results of a modeling of emergent spectra from a magnetized hydrogen atmosphere of a NS (see e.g. Zavlin, Shibano & Pavlov 1995). We must note that there is a qualitative difference between the profiles shown in Figure 3, that should manifest itself in the resulting pattern of contours of constant X-ray pulsed fraction in the α - ζ map (see § 4). The profile shown in Figure 3 by a solid line (case 1) has a substantial pencil component (of angular half-width of $\sim 15^\circ$) superposed on a relatively weak fan component, while the profile shown by a dotted line (case 2) has a very narrow (of angular half-width of $\sim 3^\circ$) pencil beam on top of a larger fan component. For case 1, the contribution of the beamed component to the integrated X-ray flux is substantial, and one can expect that the X-ray pulsed fraction and pulse width in this case will be determined by the beamed component. On the contrary, for case 2 the contribution of the beamed component is rather small, and both the X-ray pulsed fraction and pulse width will be mostly determined by the fan component. In our calculations we assume that the surface effective temperature (at the magnetic pole) and polar value of the magnetic field strength are respectively, 5×10^5 K (Geminga), 10^6 K (Vela and PSR 0656+14) and $\sim 3 \times 10^{12}$ G (Geminga), $\sim 6 \times 10^{12}$ G (Vela and PSR 0656+14). For both

these cases in our calculations we used the value $\chi_0 = 0.3$.

As has been noted by Page (1995), the response of the ROSAT PSPC results in a distortion of the observed pulsed fractions due to the mixing of photons with different energies in the detector. Photons of different energy also suffer varying degrees of interstellar absorption. The result of these effects is an increase in the observed pulsed fraction (up to $\sim 70 - 80$ %) at lower energies. In our modeling we have not included a detector response function (we assume a “perfect” detector) or interstellar absorption effects, so that the calculated pulsed fractions (at the energy of 0.18 keV) may be systematically lower than those calculated including these effects.

4. RESULTS OF NUMERICAL CALCULATION

In our calculations we use the following more or less generally accepted definition of pulsed fraction, that is sometimes also referred to as the modulation index (for a given photon energy):

$$f_{\text{pulsed}} = \frac{F_{\text{max}} - F_{\text{min}}}{F_{\text{max}} + F_{\text{min}}}, \quad (7)$$

where F_{min} and F_{max} are the minimum and maximum values of the photon flux. We define the pulse width (or FWHM) as the phase difference between the right and left wing of the pulse at half maximum (at $F_{\text{max}}/2$).

In Figure 4 we illustrate our calculations of the X-ray pulsed fraction (in %) (left panel) and pulse width (right panel) for the case of isotropic emission. In our calculations we have assumed the stellar effective temperature (at the magnetic pole) of 5×10^5 K. The results of our calculations are in reasonable agreement with those published earlier by other authors. Figure 4 shows that for the range of X-ray pulse widths of 0.35-0.5 (matching the observed ones) the pulsed fraction (at the energy of 0.18 keV) hardly exceeds a few percent. Also, Figure 4 indicates that the pulse width decreases as the pulsed fraction increases. Perhaps this tendency was one of the motivations for modeling Geminga’s X-ray emission (see Page 1995) in terms of the orthogonal rotator with highly non-dipolar magnetic field, because the former favors largest pulsed fractions while the latter may broaden the pulse (for an appropriately chosen combination of magnetic multipoles).

The principal result of our calculations is that the observed thermal X-ray light curves and profiles can be produced by an anisotropic emission pattern even for small obliquity angles. In Figure 5 we present the X-ray light curves calculated for the emission patterns with different contributions from the beamed component. The left panel in Figure 5 illustrates the light curves calculated for the emission pattern shown in Figure 3 by a solid

line (case 1) for different angles α and ζ (solid line: $\alpha = \zeta = 10^\circ$, dotted line: $\alpha = 15^\circ$, $\zeta = 50^\circ$, and dashed line: $\alpha = \zeta = 90^\circ$). The right panel in Figure 5 illustrates the light curves calculated for the fixed angles $\alpha = \zeta = 15^\circ$ and for three different cases of emission pattern where, respectively, the beamed component dominates (solid line), beamed component is suppressed (dotted line), and where the contributions from the beamed and fan components are that given in Figure 3 by a solid line.

Figures 6 - 9 summarize the results of our modeling of the soft X-ray and hard γ -ray emission for Geminga and Vela (the results obtained for Vela also apply to PSR 0656+14), respectively. Figures 6 and 8 correspond to the case of the X-ray emission pattern shown in Figure 3 by a solid line (case 1), while Figures 7 and 9 correspond to the case-2 emission pattern (Figure 3, dotted line). The calculations presented in Figures 6, 7 and 8, 9 have been performed for the effective stellar temperatures (at the magnetic pole) of 5×10^5 and 10^6 K, respectively. In Figures 6 - 9 the left and right panels display the calculated X-ray pulsed fractions (%) and pulse widths, respectively. The shaded areas in the left panels of Figure 6, 8 and 9 denote the range of the observed pulsed fractions. Our modeling of Geminga's X-ray emission (Figures 6 and 7) shows that the pulsed fractions calculated for the emission pattern shown in Figure 3 by a dotted line (case 2) are well below the observed ones. Thus, at least for Geminga, the surface X-ray emission should have a rather strongly beamed component.

Note that for the case-1 X-ray emission pattern (Figure 3, solid line) and for $\alpha \sim \zeta$ the pulse width gets smaller than 0.3 at $\alpha \sim \zeta \gtrsim 20^\circ$, while for the case-2 emission pattern this already occurs at $\alpha \sim \zeta \gtrsim 10^\circ$. This can be easily understood in terms of different angular widths of the beamed component of the X-ray emission patterns shown in Figure 3. Also, Figures 6 - 9 show that the curvature of contours of equal X-ray pulsed fraction and pulse width is determined by the angular width of the beamed component, whereas the values of the X-ray pulsed fraction and pulse width are determined by the relative contribution of the beamed component (besides a general contribution determined by the input parameters such as the effective temperature, photon energy, stellar mass and radius, etc).

Our calculations show that if one of the angles α and ζ is $\gtrsim 15 - 20^\circ$, then the contours labelling the observed values of pulse width (0.35 - 0.5) have no overlap with those labelling pulsed fraction of $> 10-20\%$. This means that our modeling of the X-ray pulsed emission alone already constrains the angles α and ζ to the small values of $\lesssim 30^\circ$. This tendency gets more pronounced for the case of a sharp pencil beam component (see Figures 7 and 9, right panels). In this case the contours of constant pulsed fraction (of $\gtrsim 10\%$) degenerate into very elongated parabolas symmetric about the diagonal $\zeta = \alpha$ and with the vertices in the low-left corner. This implies that the relatively high observed pulsed fractions (of

order of 10-20%) and large pulse widths (of order of 0.35 -0.5) may be allowed only for the relatively small obliquity and observer angles, $\alpha, \zeta \lesssim 10^\circ$. Thus, the main qualitative result of our modeling of the soft thermal X-ray emission from Geminga, Vela, and PSR 0656+14 is that the presence of a pencil component in emission is necessary and constrains the observer and obliquity angles to small values, and that the sharper a pencil component is, the closer these angles are to each other.

Figures 6 and 7 show that only the broad beam pattern (case 1) will produce a pulse fraction high enough to account for Geminga’s observed pulse fraction. The pulse width contours in Figure 6 matching the observed range of pulse widths (0.35 ± 0.05) also overlaps the allowed phase space of pulse fraction. Figure 8 and 9 show that there is allowed phase space of pulse fraction for both beaming patterns for Vela and PSR 0656+14, but the larger observed pulse widths of these pulsars is consistent with only the broad beam pattern (case 1) in Figure 8. A larger pencil beam component therefore seems to be favored for all three sources.

Assuming values of the opening angle for the hollow-cone γ -ray emission allows us to quantitatively and independently estimate the angles α and ζ for these pulsars. The contours of constant α and ζ in the hollow-cone emission model for the observed values of $\Delta\phi$ for these pulsars, shown by dashed lines in Figures 6 - 9, constrains both α and ζ to be small. For particular model parameters we employ in this paper these angles should be $\lesssim 20^\circ - 30^\circ$. This constraint from modeling the γ -ray pulse profiles is thus in agreement with those derived from modeling of the X-ray profiles. From the combined requirements of large X-ray pulsed fraction ($f_{\text{pulsed}} > 10\% - 30\%$), X-ray pulse width (0.35 - 0.5) and γ -ray pulse separation, the γ -ray beam hollow-cone opening angles must be $13^\circ \lesssim \theta_\gamma \lesssim 30^\circ$ for Geminga and $5^\circ \lesssim \theta_\gamma \lesssim 30^\circ$ for Vela.

If the pulsed thermal soft X-ray emission from Geminga, Vela, and PSR 0656+14 is dominated by a beamed component (produced e.g. by the effect of anisotropic opacity of a magnetized atmosphere), then the model X-ray light curves for these pulsars agree very well with the observed pulsed fractions and pulse widths of their soft X-ray emission (at a median energy of 0.18 keV). The calculated γ -ray profiles match the observed pulse spacing, $\Delta\phi$, for these pulsars. The simultaneous modeling of the soft (thermal) X-ray and γ -ray emission for Geminga, Vela, and PSR 0656+14 constrains the phase space for the possible obliquity and observer angles, and favors relatively small values for these angles (Figures 6 - 9).

5. SUMMARY

We have discussed the issue of whether the observed γ -ray emission and recently detected soft (presumably thermal) X-ray emission from Geminga, Vela and PSR 0656+14 can be understood in terms of a polar cap (or hollow cone) model proposed for the γ -ray emission from pulsars. We have calculated the range of observer and obliquity angles allowed by the observed pulsed fractions and widths of the soft X-ray profiles of these pulsars (at the median energy of ~ 0.18 keV), assuming anisotropy of the X-ray emission in a magnetized atmosphere. We found that small values of observer angle and obliquity are required to account for the single, relatively broad (with a phase width of ~ 0.35 - 0.5) X-ray peaks and these values can still produce the observed pulsed fractions of the X-ray profiles. The range of these angles restricted by the X-ray profiles are found to be consistent with those values required to reproduce the observed narrow double γ -ray peaks separated by a phase interval of 0.4 - 0.5 . In addition, the appearance of a single broad X-ray pulse between the two γ -ray peaks predicted by polar cap models seems to be borne out at least for Vela and Geminga.

Our main results can be summarized as follows.

1. The possibility of beaming of the thermal X-ray emission in Geminga, Vela, and PSR 0656+14 provides a consistent explanation for their observed X-ray light curves and is in accord with the polar cap models for their γ -ray emission.
2. The obliquity and/or observer angle in Geminga, Vela, and PSR 0656+14 may be less than 30° . The γ -ray opening angles must be at least 13° for Geminga and at least 5° for Vela and PSR 0656+14.
3. For anisotropic X-ray emission, the observed pulsed fraction and pulse width are much less sensitive to the effective temperature and are determined primarily by the degree of a beaming.
4. The magnitude of X-ray pulsed fraction is mainly determined by the magnitude of the beamed emission relative to the fan beam emission. In the case of a very strong beamed component, whose contribution to the X-ray flux is significant, the maximum pulsed fractions should be observed for a rather wide range of obliquity and observer angles.
5. The range of observer and obliquity angles allowing for the largest possible pulsed fraction is determined by the angular width of the beamed component. In the case of a very narrow beamed component, the maximum pulsed fractions will be observed when the obliquity and observer angles are very close to each other.

Recently, Tauris & Manchester (1998) have reanalyzed radio pulsar polarization data to compute the obliquity distribution of the parent population of all radio pulsars. Their derived distribution peaks at small obliquities and suggests that most pulsars have $\alpha \lesssim 35^\circ$. Our results are thus consistent with this picture.

There are several important issues that we have thus far not addressed in our modeling of X-ray and γ -ray pulse profiles: polar cap heating and plausible physical reasons for the observed phase offset between X-ray and γ -ray pulses. Since the pioneering study by Ruderman & Sutherland 1975 it has been understood that the development of electron-positron cascades above the NS surface initiated by primary electrons should unavoidably result in precipitation of ultra-relativistic positrons on the stellar surface. The kinetic energy of these positrons should be eventually transformed into the thermal energy of the NS crust and then reradiated most likely in soft X-rays (see e.g. Arons & Scharlemann 1979, and Arons 1981). The polar cap heating could thus add a component to the thermal X-ray pulse profiles. The efficiency of the polar cap heating depends on the number density of positrons that flow back from the pair formation front (PFF) to the stellar surface. This number density cannot be calculated from first principles. Instead it is rather sensitively determined by the transverse and longitudinal structure of the PFF, electrostatics of the PFF, and by the dynamics of positron acceleration (Harding & Muslimov 1997b). Estimates of X-ray luminosity due to polar cap heating by Arons (1981) predict that such heating accounts for only 8%, 0.12% and 0.005% of the observed thermal X-ray luminosity of Vela, Geminga and PSR 0656+14, respectively (Harding 1995).

However, these polar cap heating estimates need to be revised using more recent calculations of the electric fields above the polar cap (Muslimov & Tsygan 1990, 1992, and Muslimov & Harding 1997). We can make the following rough estimates based on the results of the general relativistic treatment of the acceleration of the primary beam over the polar cap. The main difference between this and the classical treatment (see also Arons 1996) is that the general-relativistic dragging of inertial frames allows very efficient acceleration even for an aligned rotator and does not require the concept of “favorably curved field lines” introduced by Arons & Scharlemann 1979. In the regime of the space-charge-limitation of current, the electric field in the region of electron acceleration is determined by the difference between the local charge density of electrons and Goldreich-Julian charge density $\Delta\rho_e$. This difference reaches a maximum $|\Delta\rho_e|_{\max} \sim |\rho_{\text{GJ}}|\kappa$ (where $\kappa \approx 0.38r_g/R \sim 0.15$, r_g is the stellar gravitational radius, see e.g. Muslimov & Harding 1997) at some height h_m above the surface and then exponentially declines toward the PFF. The backflowing positrons enter a regime of relativistic motion near h_m , where $|\Delta\rho_e| \sim |\Delta\rho_e|_{\max}$. The backflowing positrons tend to reduce the difference $|\Delta\rho_e|$ and therefore the maximum value of the electric field. Thus, the maximum charge density of backflowing positrons can be

estimated as $|\Delta\rho_p| \sim |\Delta\rho_e|_{\max}$. The total power put in the acceleration of these positrons can be estimated as (see also Muslimov & Harding 1997) $L^+ \sim f L_{\max}^-$, where L_{\max}^- is the maximum power of primaries, and $f \approx 0.25\kappa$. Since $L_{\max}^- \sim L_\gamma$, we get that $L^+ \sim f L_\gamma$. For a canonical NS of mass $1.4 M_\odot$ and radius 10 km we get the values L^+ that may account in part for the observed soft X-ray fluxes from pulsars (see e.g. Becker & Trümper 1997).

We now discuss the possible explanation for the phase offset (by about 0.15 in phase) of the X-ray pulse center toward the trailing γ -ray peak, observed in Geminga and Vela (see § 2). In the framework of the polar cap model, the phase offset might be explained in terms of e.g. 1) an offset dipole 2) asymmetric polar cap heating and/or 3) dragging of photon geodesics by the gravitational field of a rotating body (see e.g. Misner, Thorne, & Wheeler 1973). For the offset dipole, the geometrical vertex of the γ -ray emitting cone projects onto the stellar surface at a point offset from the magnetic pole. This means that the phase of the thermal X-ray emission (centered at the magnetic pole) will be offset from the γ -ray pulses. A significant polar cap heating component may add to the thermal X-ray profile caused by cooling. If the heating by precipitating particles is not uniform over the polar cap, then the resulting X-ray component may add more at the trailing edge of the thermal pulse. We have not yet made a detailed calculation of the distribution of heating rates over the polar cap, so this effect is hard to predict at present. Any offset due to asymmetric particle heating might be enhanced by an asymmetric γ -ray precipitation on the stellar surface near the polar cap from downward cascades due to positron acceleration. The effect of frame dragging on the light rays results in a phase shift of both X-ray and γ -ray pulses. However, since the magnitude of this effect has not been accurately evaluated and is beyond the scope of this paper, we cannot say whether this effect will quantitatively account for the observed phase offset for a 0.1-0.3 s pulsar.

In forthcoming publications we plan to discuss these and other effects in more detail and present more comprehensive theoretical analysis of the observed X- and γ -ray emission from Geminga, Vela, PSR 0656+14, and other pulsars from this subpopulation of radio pulsars.

We thank George Pavlov for discussion, and Dany Page and Slava Zavlin for providing a sample of data to test our numerical code. We are also grateful to Dave Thompson for providing us with his compilation of observed γ -ray and X-ray pulse profiles. A.K.H. acknowledges support through a NASA Astrophysics Theory Grant.

REFERENCES

- Anderson, S. B., et al. 1993, *ApJ*, 414, 867
- Arons, J. 1981, in *IAU Symp. 95, Pulsars*, eds W. Sieber & Wielebinski (Dordrecht: Reidel), p. 69
- Arons, J. 1996, *A&AS*, 120, 49
- Arons, J., & Scharlemann, E. T. 1979, *ApJ*, 231, 854
- Becker, V., & Trümper, J. 1997, *A&A*, 326, 682
- Cohen, R., Lodenquai, J., & Ruderman, M. 1970, *Phys. Rev. Lett.*, 25, 467
- Daugherty, J. K., & Harding A. K. 1994, *ApJ*, 429, 325
- Daugherty, J. K., & Harding A. K. 1996, *ApJ*, 458, 278
- Finley, J. P. 1997, private comm.
- Finley, J. P., Ögelman, H., & Kiziloğlu, Ü. 1992, *ApJ*, 394, L21
- Greenstein, G., & Hartke, G. J. 1983, *ApJ*, 271, 283
- Greiveldinger, C., et al. 1996, *ApJ*, 465, L35
- Halpern, J. P., & Wang, Y.-H. 1997, *ApJ*, 477, 905
- Harding, A. K. 1995, in *Millisecond Pulsars: A Decade of Surprises*, ed. A. S. Fructer, M. Tavani & D. C. Backer (New York:AIP), p. 322.
- Harding, A. K., & Muslimov, A. G. 1997a, in *Proc. of the 4th Compton Symposium*, eds C. Dermer, M. S. Strickman, & J. D. Kurfess, (New York: AIP), p. 648
- Harding, A. K., & Muslimov, A. G. 1997b, in preparation
- Kaminker, A. D., Pavlov, G. G., & Shibanov, Yu. A. 1982, *Ap&SS*, 86, 249
- Kanbach, G., et al. 1994, *A&Ap*, 289, 855.
- Lodenquai, J., Canuto, V., Ruderman, M., & Tsuruta, S. 1974, *ApJ*, 190, 141
- Meyer-Hasselwander, H. A., et al. 1994, *ApJ*, 421, 276.
- Miller, M. C., Lamb, F. K. & Psaltis, D. 1997, *BAAS*, 190, 36.04.

- Misner, C. W., Thorne, K. S., & Wheeler, J. A. 1973, *Gravitation*, (San Francisco: W. H. Freeman)
- Muslimov, A. G., & Harding, A. K. 1997, *ApJ*, 485, 735
- Muslimov, A. G., & Tsygan, A. I. 1987, *Sov. Astron.*, 30, 567
- . 1990, *AZh*, 67, 263
- . 1992, *MNRAS*, 255, 61
- Ögelman, H. 1995, in *The Lives of the Neutron Stars*, eds. A. Alpar, Ü. Kiziloğlu, & J. van Paradijs, (Dordrecht: Kluwer), p. 101
- Ögelman, H., Finley, J. P., & Zimmerman, H. 1993, *Nature*, 361, 163
- Page, D. 1995, *ApJ*, 442, 273
- Pavlov, G. G., Shibano, Yu. A., Ventura, J., & Zavlin, V. E. 1994, *A&A*, 289, 837
- Pavlov, G. G., & Yakovlev, D. G. 1977, *Astrofizika*, 13, 173
- Pechenick, K. R., Ftaclas, C., & Cohen, J. M. 1983, *ApJ*, 274, 846
- Ramanamurthy, P. V. et al. 1996, *ApJ*, 458, 755.
- Riffert, H., Mészáros, P. 1988, *ApJ*, 325, 207
- Ruderman, M., & Sutherland, P. G. 1975, *ApJ*, 196, 51
- Shibano, Yu. A., Zavlin, V. E., Pavlov, G. G., & Ventura J. 1992, *A&A*, 266, 313
- . 1995, in *17-th Texas Symposium on Relativistic Astrophysics*, eds. H. Bohringer, G. Morfill, & J. Trümper, *Annals of New York Academy of Sciences*, **759**, p. 291
- . 1995, in *The Lives of the Neutron Stars*, eds. A. Alpar, Ü. Kiziloglu, & J. van Paradijs, (Dordrecht: Kluwer), p. 91.
- Silant'ev, N. A., & Yakovlev, D. G. 1980, *Ap&SS*, 71, 45
- Strickman, M., Harding, A. K., & De Jager, O. 1998, submitted to *ApJ*
- Sturmer, S. J. & Dermer, C. D. 1994, *ApJ*, 420, L79
- Tauris, T. M., & Manchester, R. N. 1998, *MNRAS*, in press

Thompson, D. J. 1997, private comm.

Thompson, D. J. 1996, in Pulsars: Problems and Progress, IAU Coll. 160, eds. S. Johnston, M. A. Walker & M. Bailes

Tsuruta, S., Canuto, V., Lodenquai, J., & Ruderman, M. 1972, ApJ, 176, 739

Zavlin, V. E., Pavlov, G. G., Shibano, Yu. A., & Ventura, J. 1995, A&A, 297, 441

Zavlin, V. E., Shibano, Yu. A., & Pavlov, G. G. 1995, Astron. Lett. 21, 149

Table 1. Observed Characteristics and Model Parameters

Pulsar	Observations				Model	
	B_p (10^{12} G)	T (10^5 K)	f_{pulsed}	$\Delta\phi$	T_p (10^5 K)	B_p 10^{12} G
Geminga	3.3	5.6 ± 0.6 ^a	20-30%	0.5	5	3
Vela	6.7	15-16 ^b	11%	0.4	10	6
PSR 0656+14	9.3	8 ^c	7% ^d	?	10	6

^aHalpern & Wang 1997

^bÖgelman, Finley, & Zimmerman 1993

^cGreiveldinger et al. 1996

^dFinley, Ögelman, & Kiziloğlu 1992; Anderson et al. 1993

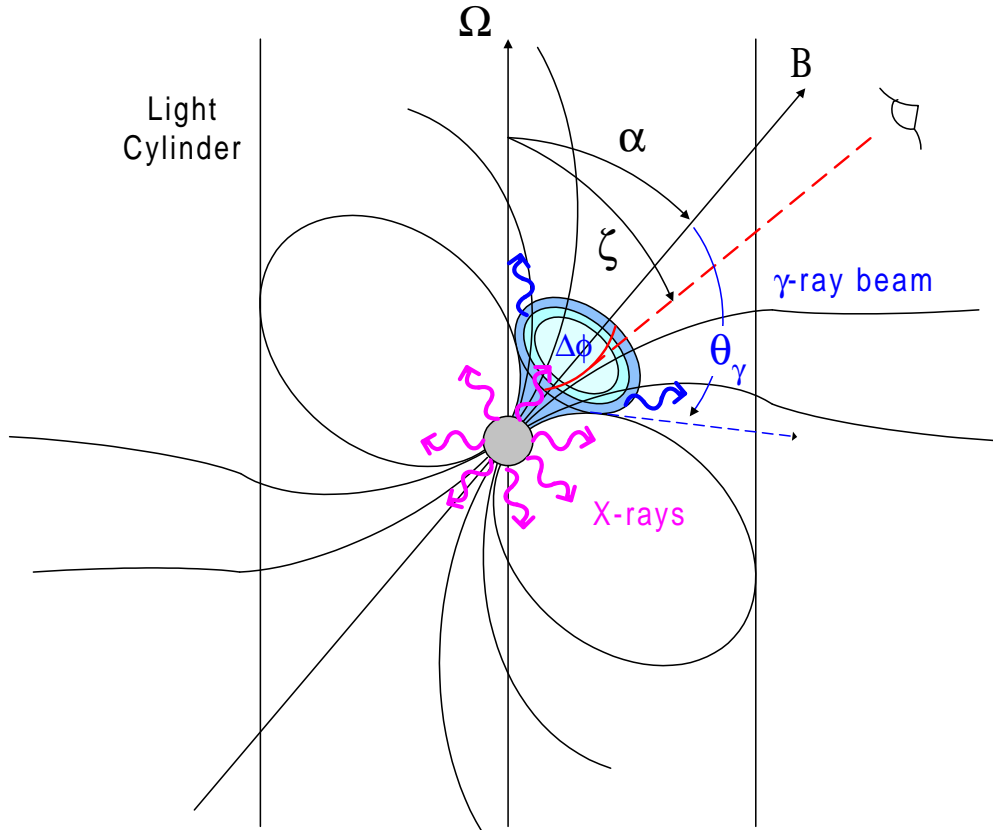


Fig. 1.— Schematic illustration of a polar cap γ -ray beam geometry. Here $\mathbf{\Omega}$ and $\mathbf{\mu}$ are the vectors of stellar angular velocity and magnetic moment, respectively. The angles α , ζ , and θ_γ specify the obliquity, observer angle, and half-opening angle of a γ -ray emitting hollow cone, respectively. The phase separation between the γ -ray pulses is $\Delta\phi$.

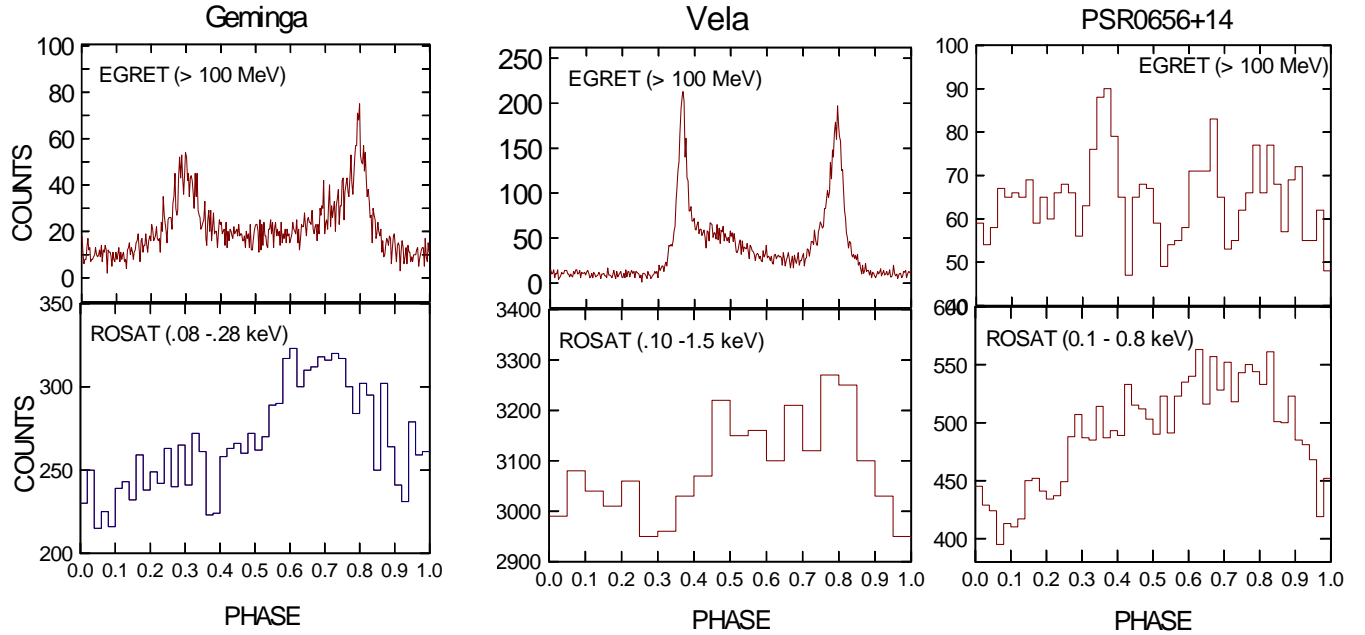


Fig. 2.— Observed X-ray (lower plots) and γ -ray (upper plots) light curves for Geminga (a), Vela (b), and PSR 0656+14 (c). See § 2 for details.

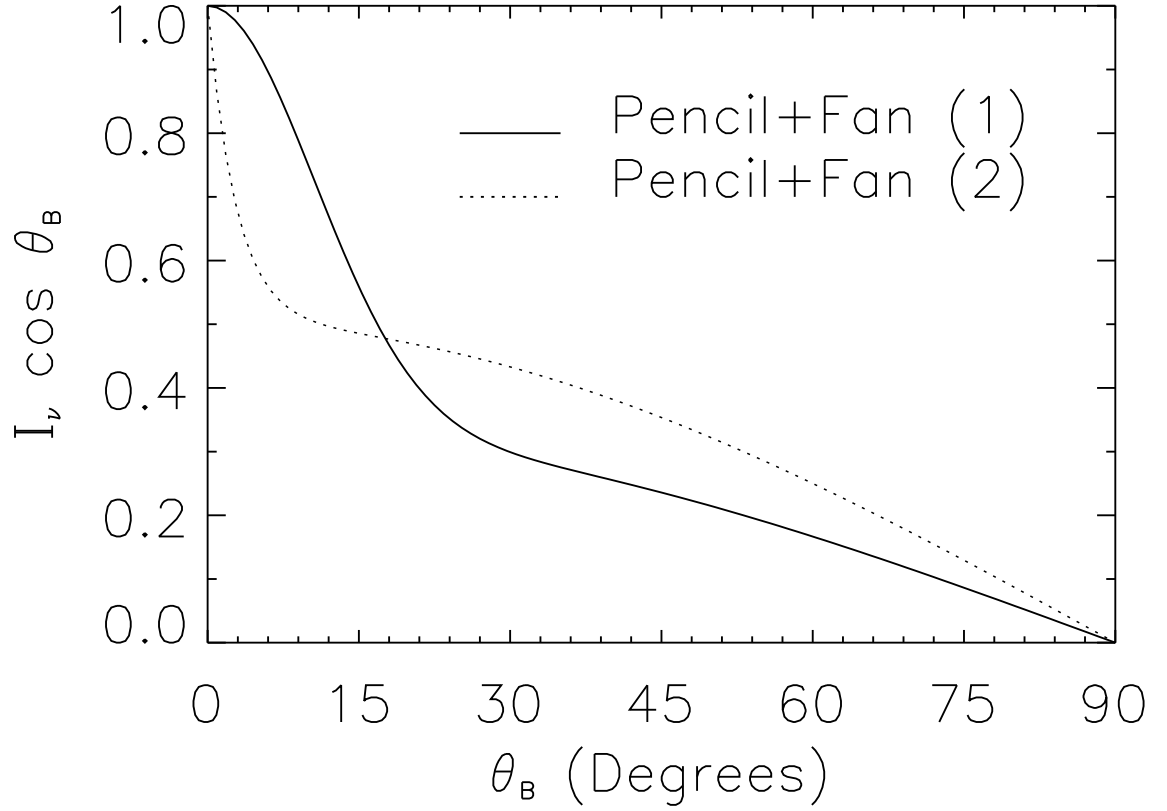


Fig. 3.— Two different profiles assumed for the anisotropic distribution of thermal X-ray emission (see § 3.1 for details). Here θ_B is an angle between the wave vector and tangent to the magnetic field line at the stellar surface.

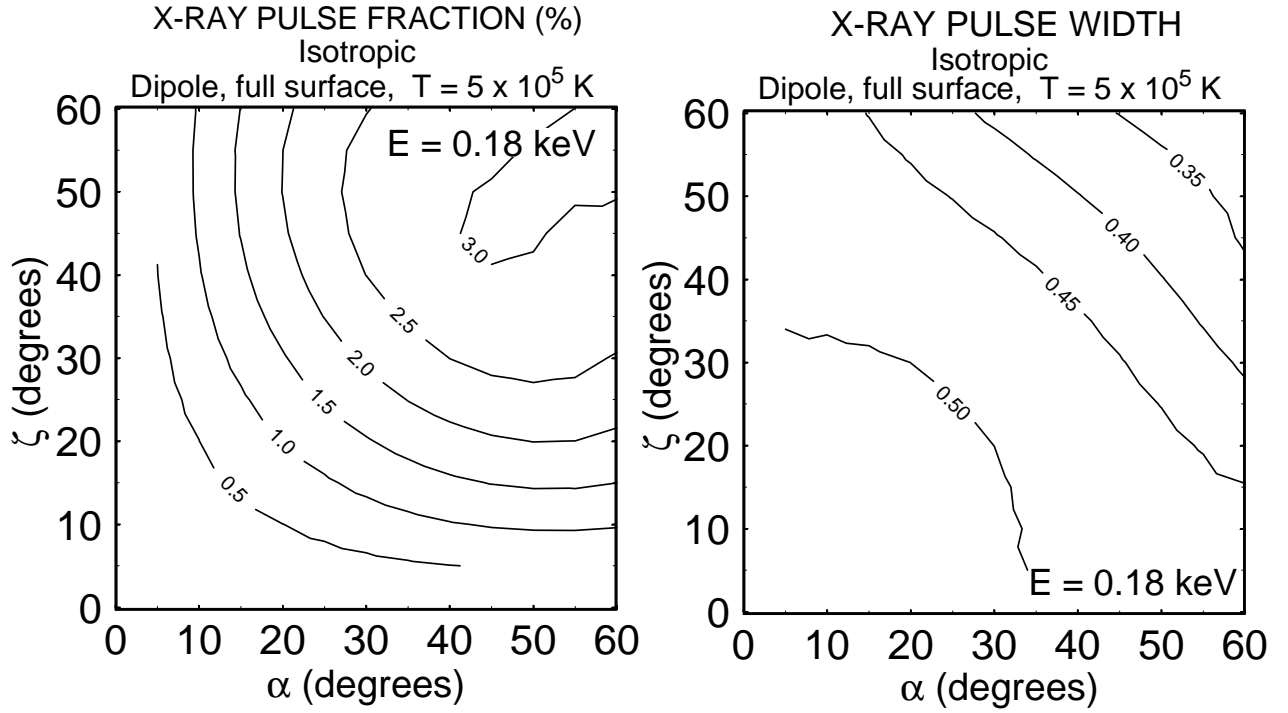


Fig. 4.— Contours of constant X-ray pulsed fraction (%) (left panel) and pulse width (right panel) for the case of isotropic emission. The calculations are performed for a dipole surface magnetic field and for the effective surface temperature at the magnetic pole of 5×10^5 K. See § 4 for details.

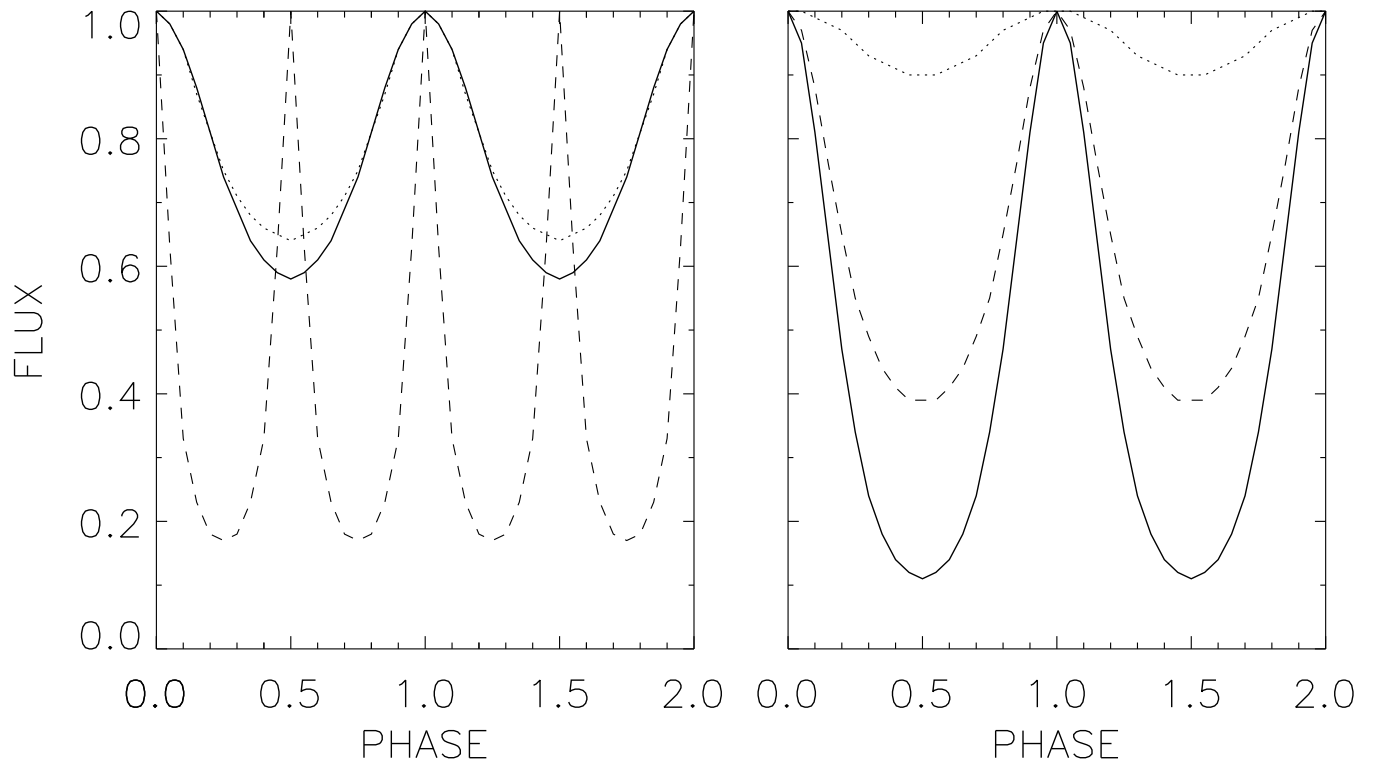


Fig. 5.— Left panel: X-ray light curves calculated for the emission profile shown in Figure 3 by a solid line and for different obliquity and observer angles (solid line: $\alpha = \zeta = 10^\circ$; dotted line: $\alpha = 15^\circ$, $\zeta = 60^\circ$; and dashed line: $\alpha = \zeta = 90^\circ$). Right panel: X-ray light curves calculated for the different emission profiles represented by the pencil (solid line), fan (dotted line), and pencil+fan (dashed line) components of the emission pattern shown in Figure 3 by a solid line and for $\alpha = \zeta = 15^\circ$. Other details are the same as in Figure 4.

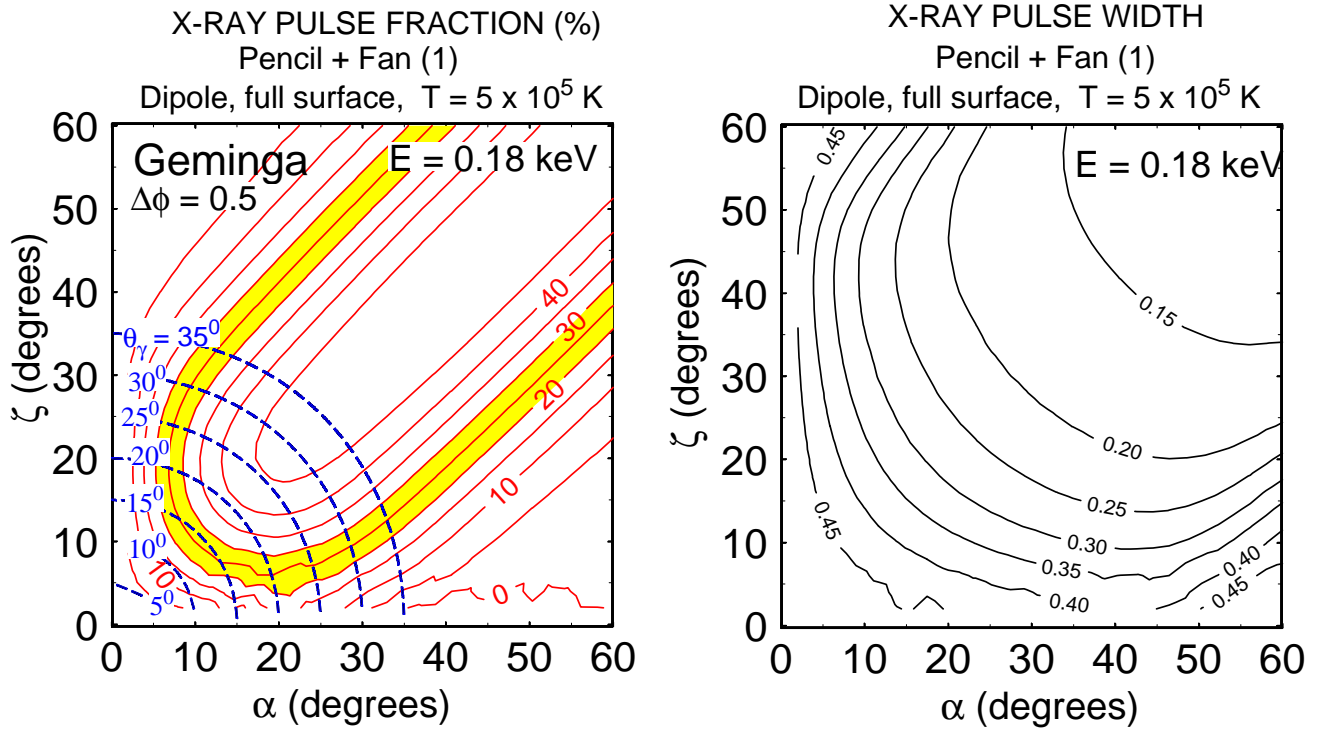


Fig. 6.— Modeling of the soft X-ray and γ -ray emission for Geminga. Left panel: contours of constant X-ray pulsed fraction (%) with shaded contours denoting observed pulsed fraction range, dashed lines are contours of constant γ -ray beam half-angle (degrees), $\Delta\phi$ is γ -ray pulse phase separation and E is X-ray energy. Right panel: contours of constant X-ray pulse width. The calculations have been performed for the X-ray emission pattern shown in Figure 3 by a solid line. The surface effective temperature (at the magnetic pole) $T = 5 \times 10^5$ K (see § 4 for details).

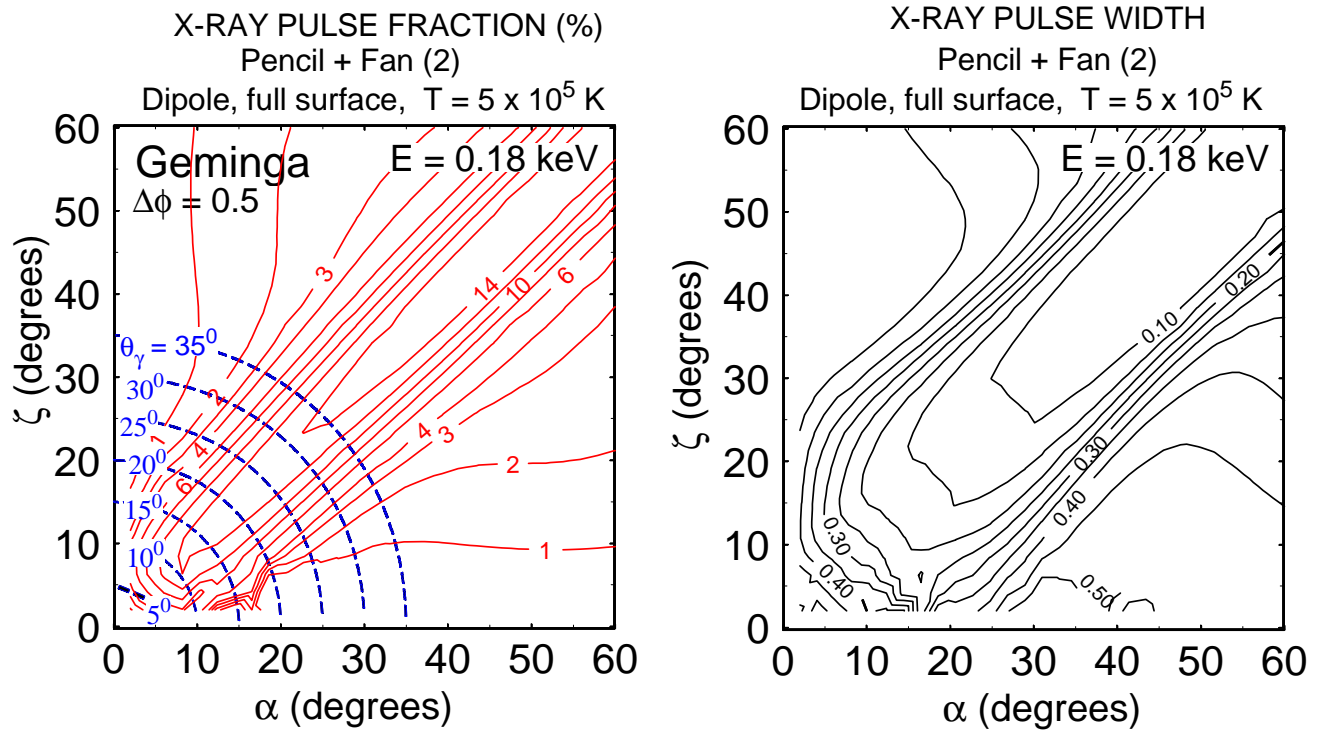


Fig. 7.— Modeling of the soft X-ray and γ -ray emission for Geminga. The calculations have been performed for the X-ray emission pattern shown in Figure 3 by dotted line. Other details are the same as in Figure 6.

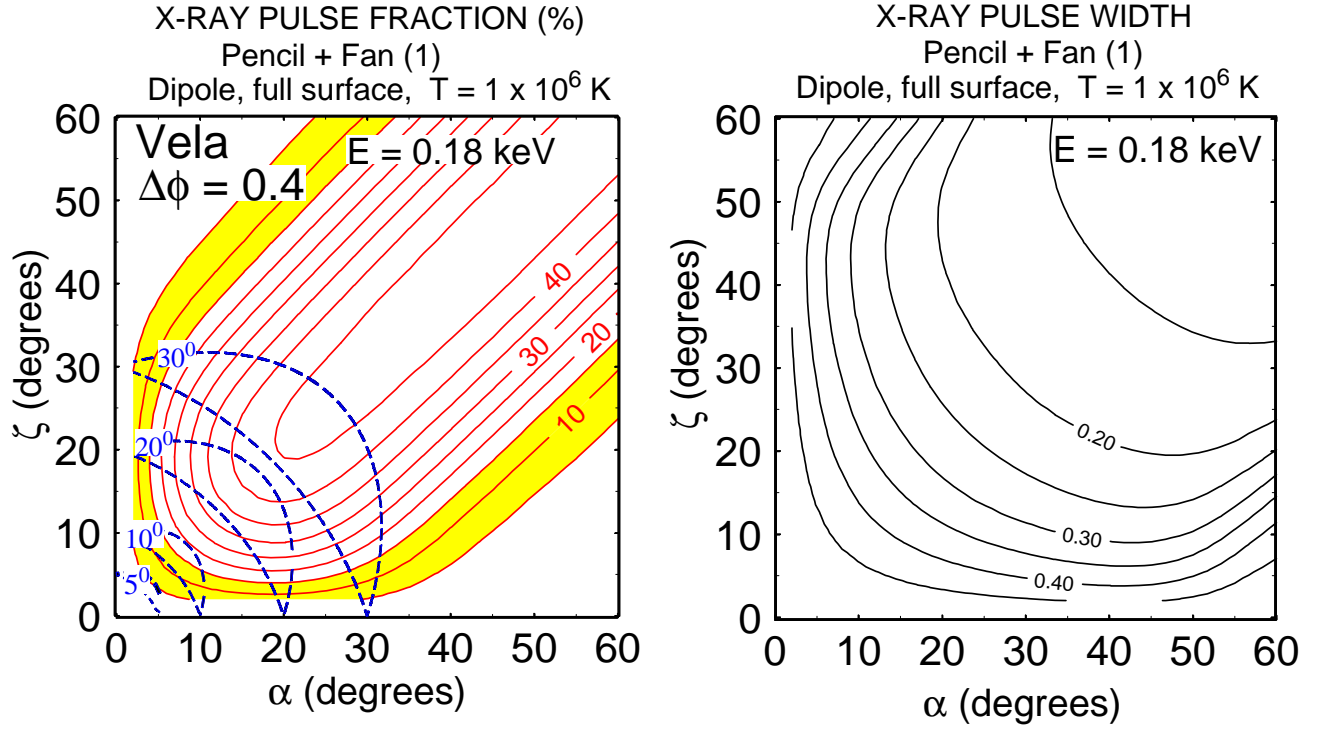


Fig. 8.— Modeling of the soft X-ray and γ -ray emission for Vela (also apply to PSR 0656+14). The surface effective temperature at the magnetic pole $T = 10^6$ K. Other details are the same as in Figure 6.

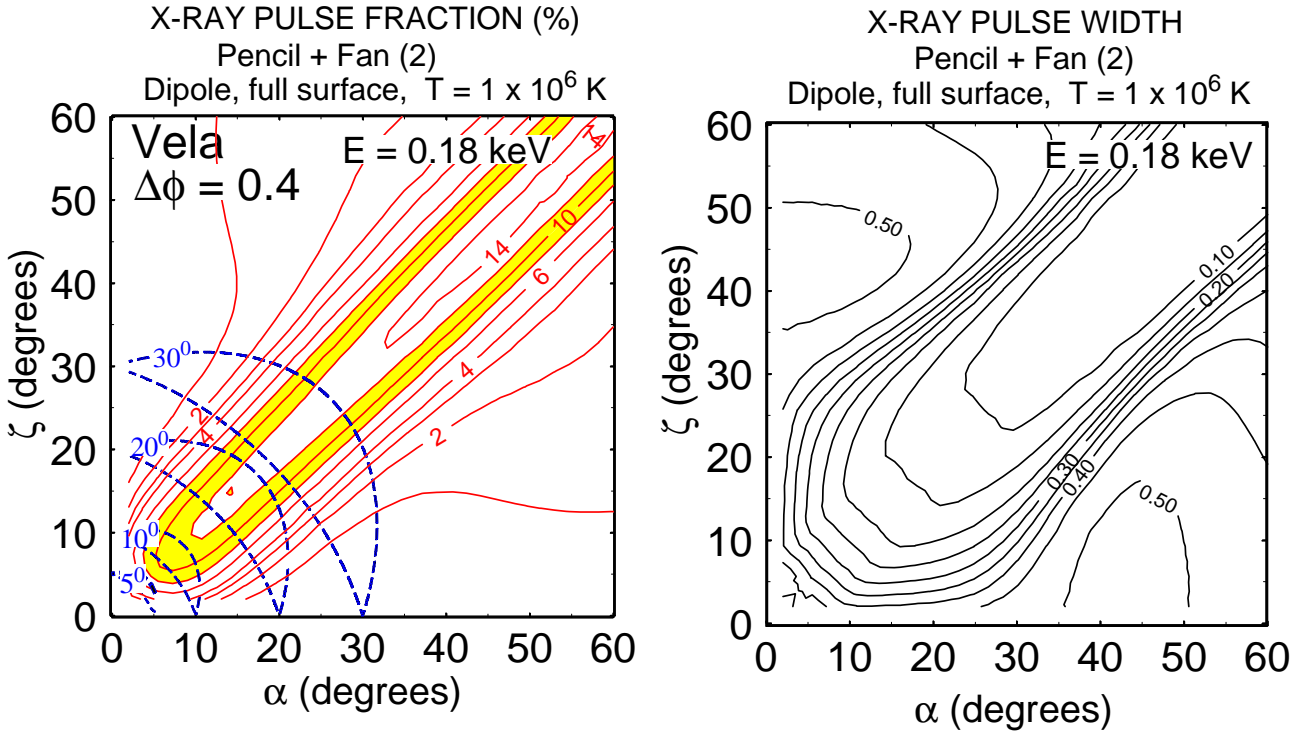


Fig. 9.— Modeling of the soft X-ray and γ -ray emission for Vela (also applies to PSR 0656+14). The surface effective temperature (at the magnetic pole) $T = 10^6$ K. Other details are the same as in Figure 7.